Tellus (1987), *39A*, 435–459

General circulation model simulation of the structure and energetics of atmospheric normal modes

By KEVIN HAMILTON, *Department of Meteorology, McGill University, 805 Sherbrooke St. W., Montreal, Quebec, Canada, H3A 2K6*

(Manuscript received 28 April; in final form 29 December 1986)

ABSTRACT

Atmospheric simulations produced by the Canadian Climate Centre general circulation model (GCM) were examined to detect Rossby normal modes such as the familiar "5-day" and "16-day" waves. Space-time spectral analysis of the simulated geopotential fields showed a concentration of power near the scales and frequencies predicted for the two gravest Rossby modes of both zonal wavenumbers one and two. By filtering the time series of simulated geopotential and wind fields in narrow bands around these spectral peaks, the vertical and meridional structures of these prominent oscillations were revealed. These structures were in good agreement with those theoretically predicted for the Rossby normal modes. The overall amplitudes of these modes appear to be realistic and even the day-to-day evolution of the modal amplitudes in the GCM is similar to that observed in the real atmosphere.

A more complicated picture emerged when the same analysis was applied to the lower frequency "16-day" wave (i.e., the second gravest symmetric Rossby mode). The spectra produced from the GCM fields failed to reproduce the peak in power in westward propagating zonal wavenumber one variance near 15–20 days that has been observed by Speth and Madden (1983). Examination of the geopotential field after it had been filtered to include only low frequency westward-propagating zonal wavenumber one variance did reveal at least one isolated episode when the meridional structure displayed some resemblance to the second gravest symmetric Rossby mode of theory. However, amplitudes are much stronger in the winter hemisphere than in the summer. A similar hemispheric asymmetry in the "16-day" wave has been found in observations.

The strength of the gravest symmetric zonal wavenumber one Rossby mode ("5-day" wave) was examined in a series of GCM simulations performed with climatological sea surface temperatures and in simulations that had anomalously warm sea surface temperatures imposed in the tropical Pacific. There is a clear tendency for the 5-day wave to be stronger in the simulations with warm ocean temperatures, in agreement with observations of the interannual variability of this mode in real data.

The excellent simulation of the gravest Rossby modes in the model suggests that the forcing and dissipation mechanisms for the modes in the GCM may also be realistic. An attempt was made to examine the forcing and dissipation of the modes in the model through a diagnostic study of the energetics of the simulated fields. The interaction with topography acts as a net sink for the modal energy. The dissipation arising from the parameterized mechanical friction in the GCM is much more important for these modes than that due to radiative heating and cooling.

1. Introduction

Spectra of observed atmospheric pressure and temperature fields are known to include substantial westward propagating variance at very large scales (e.g., Pratt and Wallace, 1976; Speth and Madden, 1983). Much of this westward propagating variance can be identified with the Rossby wave normal mode oscillations of the atmosphere (see Madden, 1979, and Salby, 1984, for reviews). Particularly evident in the data is the gravest symmetric zonal wavenumber one Rossby mode or "5-day wave" (e.g., Eliasen and Machenhauer, 1965, 1969; Madden and Julian, 1972, 1973).

Other Rossby modes that have been detected in atmospheric data include the gravest antisymmetric wavenumber one mode (the "10-day wave" of Hirota and Hirooka, 1984), the second gravest symmetric wavenumber one mode (the "16-day wave" of Madden, 1978) and the gravest symmetric wavenumber two mode (the "4-day wave" of Hirota and Hirooka, 1984). Detailed studies of the behaviour of a large number of the Rossby modes in global tropospheric analyses have been presented recently by Lindzen et al. (1984) and Ahlquist (1985).

In contrast to the large number of observational papers dealing with the Rossby normal mode oscillations of the atmosphere, there has been relatively little work concerned with the simulation of these modes in comprehensive general circulation models (GCMs). Hayashi (1974) showed that the five day wave was present in a GFDL grid point model. Tsay (1974) briefly discussed the appearance of the five day wave in a simulation produced with the NCAR GCM. Hayashi and Golder (1983a) examined the transient planetary waves simulated by a GFDL spectral GCM and found oscillations resembling the "5-day" and "16-day" Rossby modes. The present paper reports on a much more detailed examination of the normal mode oscillations appearing in the simulations produced by a state-of-the-art tropospheric/lower stratospheric GCM, namely the one developed at the Canadian Climate Centre (Boer et al., 1984a,b).

Analysis of the structure and climatology of normal modes is of interest for a number of reasons. The first of these is simply to validate the model through a comparison of the observed and simulated modal structures, frequencies, amplitudes etc. This validation of the normal mode component of GCM simulations is important both in climate modelling applications and in numerical weather forecasting. It is known that much of the forecast error in numerical prediction is associated with the misrepresentation of the external Rossby modes (e.g., Lambert and Merilees, 1978; Desmarais and Derome, 1978; Daley et al., 1981). The problems with the external Rossby modes in numerical prediction are largely caused by errors in the initial conditions, but could obviously be exacerbated if the model employed tended to a climatology with unrealistic structures or amplitudes for these modes. Another important motivation for the study of normal modes in GCMs is the possibility of performing diagnostic studies of the forcing and dissipation of the modes using the detailed results available from a model simulation.

The plan of the present paper is as follows. Section 2 briefly reviews the theory and observations of atmospheric normal modes. Section 3 presents a description of the Canadian Climate Centre GCM and of the simulations analyzed in the present investigation. Also considered in Section 3 are the modifications introduced into the theory of atmospheric normal modes by the numerical limitations of the GCM. The results obtained for the structures and time dependence of the Rossby modes in a control simulation are described in Section 4. Section 5 then considers the changes found in the modes in model simulations with anomalously warm sea surface temperatures imposed in the tropical Pacific (i.e., in GCM experiments designed to simulate the atmospheric circulation during the mature phase of a tropical El Niño event). Section 6 discusses the energetics of the Rossby normal modes appearing in the GCM simulation. The conclusions are summarized in Section 7.

2. Review of theory and observations of atmospheric normal modes

2.1. *Theory*

The study of atmospheric normal modes began with early efforts to determine the frequencies and structures of the linear free oscillations of an unforced, adiabatic, inviscid atmosphere (see Salby, 1984, for a review of the early history). The normal modes of nondivergent barotropic equations linearized about a motionless mean state were obtained by Haurwitz (1940). The corresponding three-dimensional primitive equation problem was first solved completely by Dikii (1965) and Dikii and Golitsyn (1968). They examined the "classical" problem of the free oscillations of the primitive equations linearized about a motionless mean state with temperature a function only of height. In this simple case the perturbation fields take the form of zonally-travelling waves modulated by a structure separable in height and latitude. The vertical structure of each mode is equivalent barotropic. In an isothermal mean state the vertical amplitude structure is just that of a Lamb wave (Lamb, 1932). The meridional structures of the modes can be obtained as the eigensolutions of Laplace's Tidal Equation (LTE) for a barotropic ocean of some mean depth h. The appropriate value of the "equivalent depth", h, depends on the vertical temperature structure assumed for the mean state. For realistic temperature structures the equivalent depth computed for the terrestrial atmosphere is about 10 km (Dikii, 1965; Salby, 1979). For the discretized equations used in a GCM, a slightly smaller value of h would appear to be appropriate (see Subsection 3.3 below). The horizontal structures and modal frequencies obtained as solutions of LTE have been discussed by Dikii (1965), Dikii and Golitsyn (1968) and Longuett-Higgins (1968). The classical theory predicts the existence of an infinite number of branches to the dispersion relation. Some of these branches are associated with the relatively low frequency, westward propagating Rossby modes, others represent Rossby-gravity, Kelvin and gravity normal modes. The Kelvin modes all have predicted periods less than 33 h and the gravity modes have periods less than 14 h. Most theoretical and observational work has focused on the Rossby modes, but discussions of the higher frequency normal modes can be found in Matsuno (1980), Hamilton (1984) and Hamilton and Garcia (1986).

In the present paper each Rossby mode will be labelled with two indices, (s,n), where s is the zonal wavenumber and n is a meridional mode number such that there are n-1 zero crossings in the modal pressure field from pole-to-pole. The theoretically predicted structures for the pressure perturbations associated with the first three gravest Rossby modes of $s = 1$ and $s = 2$ for a 9.36 km equivalent depth are displayed in Fig. 1. The structures for the horizontal wind perturbations are similar to those shown in Kasahara (1976).

More sophisticated theoretical studies of the Rossby normal mode oscillations of the atmosphere have been conducted by Geisler and Dickinson (1976), Schoeberl and Clark (1980) and Salby (1981a,b). They all examined the forced linear response of an atmosphere with specified dissipation and mean zonal wind structure. These studies showed that maxima in the response occurred for forcing at frequencies close to those predicted for the classical normal modes. The vertical and meridional structures of the solutions forced at these frequencies do resemble those of the classical normal modes, particularly in the troposphere. The agreement of the modal frequencies and structures in the calculations including mean winds and those in the classical theory is best for the higher frequency (i.e., gravest) Rossby modes and tends to break down seriously as modes with smaller phase speeds are considered. On the basis of his calculations, Salby (1984) suggested that the first few gravest Rossby

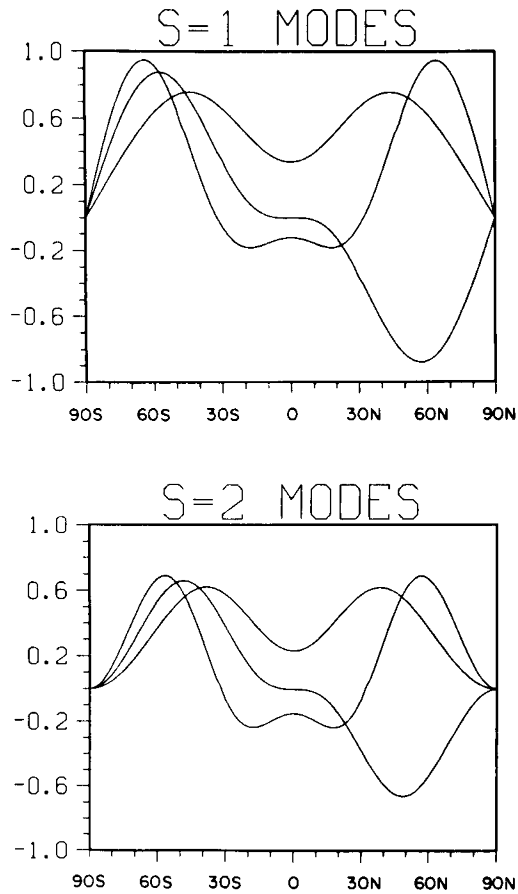

Fig. 1. Meridional dependence of the geopotential associated with the three gravest Rossby modes of zonal wavenumber one (top) and two (bottom). The normalization is the same as in Lindzen et al. (1984).

modes of zonal wavenumbers one, two and three might be present in the atmosphere in a recognizable form. Table 1 shows the theoretically predicted periods of some of these modes.

2.2 Observations

Various studies have identified many of the Rossby normal modes in the atmosphere. In this section a brief review will be given of some observational investigations that have employed techniques similar to those that were applied to the GCM output in the present study.

Eliasen and Machenhauer (1965, 1969) expanded daily 500 mb geopotential analyses in terms of spherical harmonics (some of which approximate the horizontal structures of the classical normal modes). By plotting time series of the phase determined for each day, for each harmonic, Eliasen and Machenhauer were able to demonstrate that the very large scale waves tended to propagate westward with reasonably uniform phase speeds. Dikii and Golitsyn (1968) showed that Eliasen and Machenhauer's observed phase speeds were in good agreement with those predicted by the classical theory.

Recently Lindzen et al. (1984) have performed a similar analysis, but expanding 500 mb analyses into the actual classical modes of a ten km equivalent depth atmosphere (and using both the geopotential and horizontal winds to define the modal structure). They plotted time series the daily values of both the amplitude and phase for the first few gravest modes of zonal wavenumbers one, two and three. They found fairly regular phase propagation at speeds similar to those predicted by theory, but with amplitudes that varied significantly over time scales of the order of the wave period.

Table 1. *Theoretically predicted periods of some of the largest scale Rossby normal modes in the atmosphere from Salby (1981b); the final column gives the names that have been used in the literature for the modes*

Mode	Period range (days)	Name
(1,1)	3.3–5.6	5-day wave
(1,2)	9.1–11.1	10-day wave
(1,3)	14.3–20.0	16-day wave
(2,1)	3.8–4.5	4-day wave
(2,2)	6.7–7.7	
(2,3)	11.1–20.0	

Many studies have employed space-time spectral analysis to examine the characteristics of large scale transient waves in time series of global or hemispheric analyses. Speth and Madden (1983) computed space-time spectra of geopotentials from several years of NMC analyses at various pressures and latitudes. They found distinct peaks in the spectra of westward propagating wavenumbers one, two and three that were near the predicted frequencies for each of the three gravest Rossby modes (i.e., the (1,1), (1,2), (1,3), (2,1), (2,2), (2,3), (3,1), (3,2) and (3,3) modes). Speth and Madden also examined the vertical and meridional modulation of the geopotential variance in the frequency bands associated with the "5-day" and "16-day" waves (i.e., the (1,1) and (1,3) modes). They concluded that these structures are consistent with the identification of the spectral peaks with Rossby normal mode oscillations.

Hirota and Hirooka (1984, 1985) applied space-time spectral analysis to global stratospheric geopotential fields constructed from satellite radiometer data. They then resynthesized the geopotential field associated with the westward propagating zonal waves within narrow frequency intervals near the theoretically predicted frequencies of the (1,1), (1,2), (2,1) and (2,2) Rossby normal modes. The meridional structures of the resynthesized geopotentials displayed a striking resemblence to the corresponding classical modes. Earlier, Rodgers (1976) had presented a similar analysis (although only for the (1,1) mode) of satellite radiance observations with the same results.

The identification of the relatively high frequency (1,1), (1,2), (2,1) and (2,2) modes in data has been a fairly straightforward matter. The published evidence suggests that the lower frequency (1,3) and (2,3) Rossby modes are not manifested so clearly in the atmospheric circulation, particularly around the solstices. Madden (1978) found that the spectral signals associated with the (1,3) mode were weaker in the summer hemisphere than in the winter hemisphere. Hirota and Hirooka (1985) found clear evidence for coherent global (1,3) and (2,3) modes at stratospheric levels only near the equinoxes. Daley and Williamson (1985) have examined both tropospheric and stratospheric data during January 1979 when a prominent, westward-propagating, zonal wavenumber one disturbance with period near 20 days was observed in the Northern Hemisphere. They found (at most) only a weak corresponding signal in the southern hemisphere, and they questioned whether the observations of the long period travelling wave in the northern hemisphere should be interpreted as a normal mode oscillation.

3. The GCM simulations

3.1. The model

The Canadian Climate Centre GCM employed in this study has been described in detail by Boer et al. (1984a,b), and so only a brief summary of the main features of the model will be given here. The GCM is cast in the usual spectral formulation with triangular truncation at wavenumber 20. The geopotential and horizontal wind fields are evaluated at ten sigma levels (0.010, 0.032, 0.080, 0.150, 0.235, 0.360, 0.550, 0.750, 0.880 and 0.970), with temperature and vertical velocity carried at half levels. In addition the surface pressure is explicitly calculated at each time step. The usual rigid lid boundary condition $d\sigma/dt$ is imposed at zero pressure.

The model is forced by radiative heating computed with realistic radiative transfer algorithms. Both the long-wave and short-wave radiation codes consider the effects of water vapour, ozone, carbon dioxide and clouds. Ozone and cloud distributions are specified from climatological values. The solar zenith angle in the shortwave heating calculation undergoes both diurnal and annual variations. Parameterizations are included of small scale physical processes, such as moist convection and surface drag. A somewhat unusual feature of this GCM is the inclusion of parameterized vertical momentum fluxes associated with subgrid scale gravity waves. In the version considered here the sea surface temperatures (SSTs) are imposed, while the surface temperatures over land areas are computed from the surface energy budget.

3.2. The experiments

In the present study, the most detailed analysis was performed using a 120-day segment (November 1–February 28) from the middle of a five year control simulation with climatological SSTs (Boer et al., 1984b). In this run the wind, temperature, geopotential, precipitation, radiative heating and surface flux fields were saved to tape every 6 h.

Further analysis was performed on simulated fields from a series of model experiments that were originally conducted at the Canadian Climate Centre to gauge the response of the GCM to tropical Pacific SST anomalies (some of this work is described in Boer, 1985). A control simulation with climatological SSTs was run for ten years. Then a number of simulations extending from October through February were performed with SST anomalies imposed in the equatorial Pacific. The SST anomaly in each case was introduced with gradually increasing amplitude through the month of October, attained its full value at the end of October, and was held constant thereafter. The SST anomalies imposed were based on a standard SST anomaly (SSSTA) which was an idealization of the composite SST anomaly of Rasmusson and Carpenter (1983) representing the mature phase of a typical El Niño/Southern Oscillation event. Four such El Niño simulations employed in the present study had two times the SSSTA imposed, and another had four times the SSSTA. The period analysed in each case was December 1–February 17. The model fields in the ten year control run were saved every 17.5 h, while in the El Nino experiments the fields were archived every 18 h (by choosing a segment 78.75 days long, the time series for the control run have 105 values, while those for the El Niño experiments include 108 values).

3.3 The normal mode oscillations of the GCM

The free oscillations supported by the discretized equations governing the evolution of the circulation in a GCM differ in some respects from those allowed by the governing equations for a continuous atmosphere. This issue has been addressed by various authors (e.g., Williamson and Dickinson, 1976). It seems clear that the horizontal resolution in a typical GCM (such as the Canadian Climate Centre model) is adequate to represent the structures of the first few gravest Rossby modes. More significant distortions of the free oscillations are introduced by the finite vertical resolution and upper boundary conditions employed in GCMs.

As part of the present project, the equation governing the vertical structure of the modes in the classical linear theory was solved numerically using centred differencing on a numerical grid with levels at 1000, 970, 880, 750, 550, 360, 235, 150, 80, 32, and 10 mb (corresponding roughly to the sigma surfaces in the GCM). Boundary conditions were imposed that required the vertical velocity to vanish at 1000 mb and for the pressure perturbations to vanish at zero mean pressure. The mean temperature structure employed in these linear calculations was based on global average temperatures computed on various pressure surfaces from the 120-day segment of GCM simulation discussed above. The discretized vertical structure equation with the rigid lid boundary condition has 11 eigensolutions, each with an associated equivalent depth. The structure of the gravest solution (external mode) is shown in Fig. 2. The structure of the mode in this figure is quite similar to that of the free mode in a continuous atmosphere with realistic mean temperature structure (e.g., Salby, 1979), although the external mode in the model grid may have a slight tendency to be more strongly intensified near the top level. The solution shown in Fig. 2 is associated with an equivalent depth of 9.36 km. This is close to (but somewhat smaller than) the values that have been obtained for the free mode of a continuous atmosphere (e.g., Dikii, 1965; Salby, 1979). The slightly smaller value of the equivalent depth in the model has only a very modest effect on the frequencies and meridional structures of the classical normal modes. Calculations were performed of the eigenfrequencies of LTE corresponding to the modes listed in Table 1 when $h = 10$ km and when $h = 9.36$ km. The largest difference in the computed frequencies occurred for the (1,1) mode. In that case a period of 120.5 h was obtained for $h = 10$ km, and a period of 123.5 h with $h = 9.36$ km.

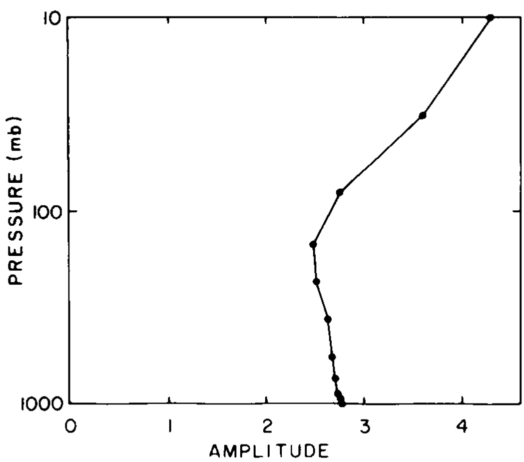

Fig. 2. The vertical structure of the geopotential variations in the external mode of the classical theory when the governing equations are discretized on a level structure similar to that employed in the Canadian Climate Centre general circulation model. The units on the amplitude axis are arbitrary. The equivalent depth associated with this mode is 9.36 km.

The other eigensolutions of the discretized vertical structure equation correspond to internal modes with differing numbers of zero crossings in the vertical. These modes exist only because of the rigid lid boundary condition and have no counterparts in the theory for a continuous, unbounded atmosphere. The internal modes are all associated with much smaller equivalent depths than the external mode (for the present calculation these modes were found to have equivalent depths of 2.43 km, 0.79 km, 0.355 km etc.). The frequencies obtained for normal modes with the internal vertical structures will be much smaller than for the corresponding external modes. This means that the internal Rossby normal modes will all have very small predicted phase speeds in the classical theory, and so probably would not be identifiable in a full model simulation. On the other hand, the theory predicts that there will be many of the internal gravity modes with phase speeds sufficiently large to be realizable under realistic conditions and that have periods of the order of a few days. Thus, in contrast to the very high frequency external gravity modes, the internal gravity modes in the model do have the potential to contribute substantially to the variability on meteorologically significant time scales.

4. Analysis and results for the control run

4.1. *Space-time spectra*

The model fields were saved at 6-h intervals in the 120-day segment of the control run analyzed as part of the present project. The fields were generated in the model in spectral form on sigma surfaces. For present purposes these values were interpolated onto latitude-longitude grids at pressure levels of 1000, 500, 250, 150, 70, 30 and 10 mb. The least-squares linear trend over the 120-day period was removed from the data at each grid point. The diurnal and semidiurnal harmonics were then filtered out of the time series at each grid point.

The time series of the 6-hourly geopotentials at individual pressures and latitudes were Fourier analyzed into eastward and westward propagating zonal waves using the method of Hayashi (1971). At a particular latitude and pressure the results can be expressed as a set of individual periodograms, one for each eastward and westward propagating zonal wavenumber. Each of these periodograms includes values for 240 Fourier frequencies (from periods of 120 days through to 12 h). Spectral estimates were constructed by taking running means of the periodograms over three consecutive Fourier frequencies (i.e., a bandwidth of 0.025 day^{-1}).

The results for westward and eastward propagating zonal wavenumber one components of the 250 mb geopotential height at six latitudes are displayed in Fig. 3. The ordinate in this figure represents power per Fourier frequency (i.e., power per frequency interval of 0.0083 day^{-1}). These results can be compared to similar spectra computed from NMC analyses presented in Fig. 6 of Speth and Madden (1983; hereafter SM). Note, however, that SM used 96-day time series, so that the present power estimates should be multiplied by 120/96 (= 1.25) in order to be comparable to SM's values.

One striking feature that appears in the comparison of the present Fig. 3 with SM's results is a general deficiency in total variance of both eastward and westward propagating waves in the model. For example, at 60° N in SM the maximum spectral estimate for westward propagating wavenumber one is about 3000 m^2, while the model results at 58.1° N have a maximum of 1400 m^2 ($\times$ 1.25 = 1750 m^2). The discrepancies between SM's observations and the model results are more pronounced at higher frequencies, particularly at frequencies greater than about 0.1 day^{-1}. The Canadian Climate Centre GCM, like most such models, is known to be deficient in total transient eddy kinetic energy (Boer et al., 1984b). The results in Fig. 3 show that this deficiency applies to the zonal wavenumber one component of the upper tropospheric flow at all frequencies, but is particularly pronounced at high frequencies.

Obvious in the spectra of westward propagating $s = 1$ variance in Fig. 3a are peaks at each latitude near a period of 5 days (i.e., frequency of 0.2 day^{-1}). This appears at virtually the same frequency as the peaks SM identified with the (1,1) Rossby mode in their observational spectra. At 58.1°N, 36.0°N, 36.0°S and 58.1°S this peak is about 20 m^2 tall, while at 19.4°N and 19.4°S the peak is about 5–10 m^2 tall. If the width of these peaks is taken to be roughly 0.05 day^{-1}, then this leads to an estimated total power in this peak of about 100 m^2 in midlatitudes and less than half of this at low latitudes. The corresponding r.m.s. amplitudes would then be of the order of 10 m in midlatitudes and somewhat smaller in the tropics. This amplitude estimate is in rough agreement with observational values that have been quoted in the literature for the 5-day wave (e.g., Madden and Julian, 1973; Ahlquist, 1985). The corresponding spectral peak in the results of SM appears to be somewhat stronger, with perhaps two or three times the power seen in the GCM spectra of Fig. 3a.

Near westward propagating periods of about 9 days (i.e., frequencies near 0.11 day^{-1}) peaks are apparent at 58.1°S and 36.0°S in Fig. 3a. This frequency corresponds to that anticipated for the gravest antisymmetric (1,2) Rossby mode (see Table 1). Unfortunately this peak is not evident at other latitudes (i.e. at low latitudes or in the winter hemisphere). It is not surprising that the signal of the antisymmetric (1,2) mode would be small in low latitudes. In SM's results, however, the spectral peak corresponding to the (1,2) mode is seen in the midlatitudes of the winter hemisphere but not in summer.

At still lower frequencies, the classical theory predicts the existence of the (1,3) Rossby mode with periods around 18 days. SM found that

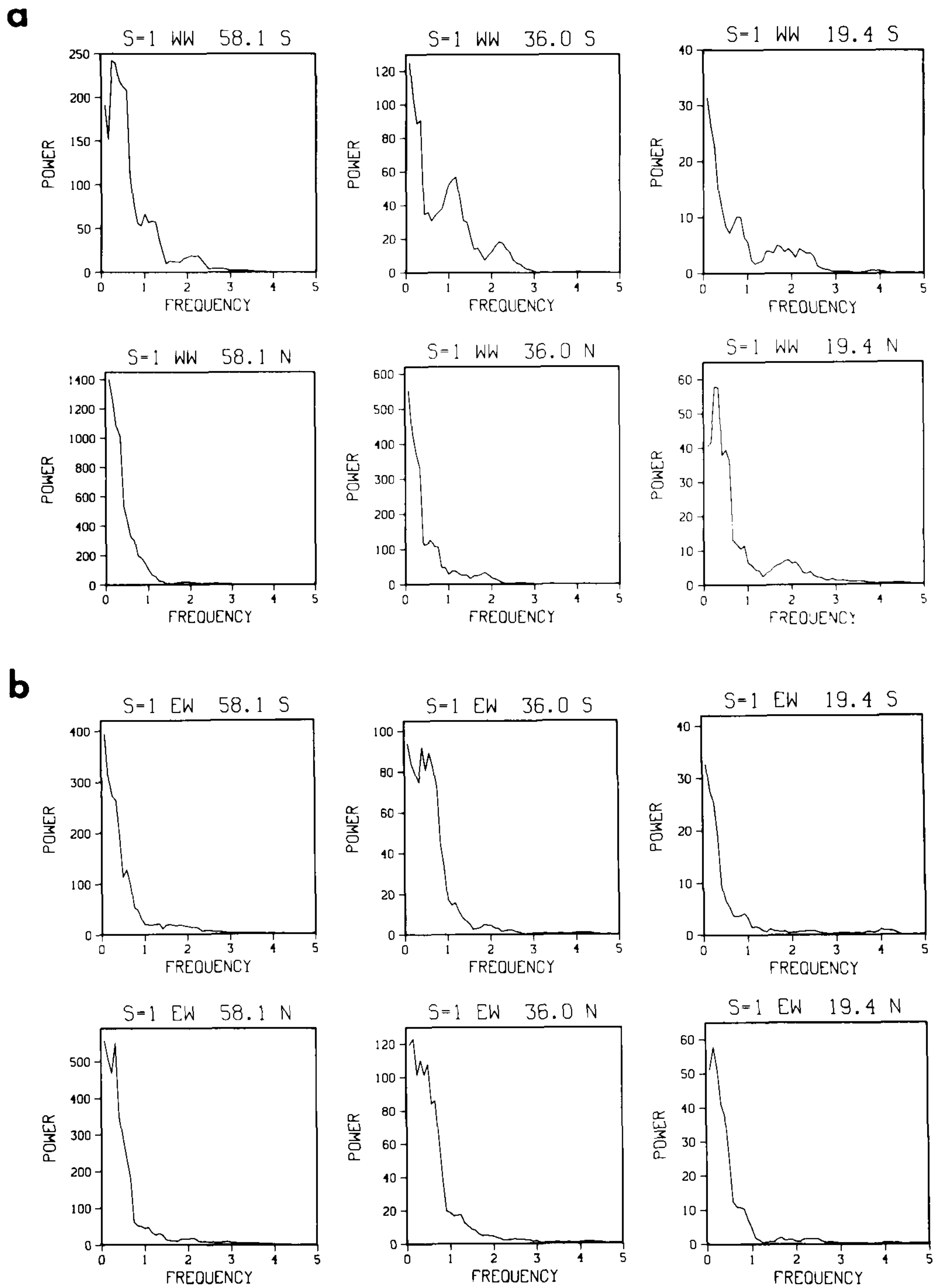

Fig. 3. (a) Spectra of westward propagating zonal wavenumber one variance of the 250 mb height field in the 120-day control run at six selected latitudes. The power axis in each panel is labelled in squared metres per Fourier frequency and the labels on the frequency axis are in 0.1 day^{-1}. (b) As in (a) but for eastward propagating variance.

poleward of about 50°N in both summer and winter distinct peaks appear centered near periods of about 15–20 days which they identify with the (1,3) mode. The model results depicted in Fig. 3a do not display peaks at this frequency and actually show either a peak at very low frequencies (~40 days) or simply a red spectrum even at the lowest frequencies.

Much of the very low-frequency power seen in the spectra of Fig. 3 may be attributable to topographically forced quasi-stationary waves. This component of the circulation is known to be strongly suppressed in the summer stratosphere. Fig. 4 shows the spectra of eastward and westward propagating variance of the wavenumber one component of the 30 mb height at 19.4°S. The red background is much less evident and the spectrum of westward propagating variance displays 2 clear peaks centred at periods of about 5 and 20 days, corresponding to the predicted periods of the (1,1) and (1,3) symmetric Rossby modes.

The spectrum of eastward propagating wavenumber one variance in Fig. 4 is also interesting. Except for a red tail at very low frequencies, almost all the power is concentrated in 2 fairly narrow peaks. One of these is centred at about 0.21 day^{-1} (a period of 4.8 days), the other at about 0.41 day^{-1} (a period of 2.4 days). These peaks are clear only in the stratosphere (e.g., compare with Fig. 3). At lower levels there may be variance associated with the same motions, but the spectral signal of such motions may be buried in the large background of eastward propagating variance. The horizontal structures of the motions associated with these peaks can be revealed by the filtering procedures described in the next section. It turns out that the 2.4-day peak is associated with an antisymmetric meridional structure and a complicated vertical structure with zero crossings at two or more levels. This suggests that the 2.4-day wave may be identified with an internal gravity mode (it should be noted here that the structures of even such relatively high frequency eastward propagating modes will be somewhat distorted by the strong mean westerlies present in the model stratosphere). The meridional structure of the motions associated with the 4.8-day peak will be discussed at the end of the following section. It appears that this disturbance has an equatorially-trapped structure, at least in the stratosphere, and may be identifiable as a Kelvin wave. The zonal wavenumber and frequency of this feature are comparable to those of the prominent internal Kelvin wave observed in the upper atmosphere by Hirota (1978).

The motions in the GCM simulation responsible for the 2.4-day peak in the spectrum of eastward propagating variance in Fig. 4 have no known counterpart in the atmosphere. If they do reflect the presence of an internal normal mode, then they would clearly be spurious components of the circulation, depending for their existence on the upper boundary condition of the model. The artificial upper boundary condition may explain the presence of these motions in the simulation, but the question of why this

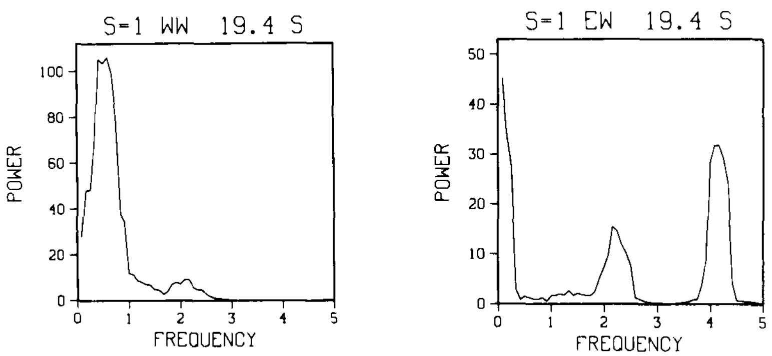

Fig. 4. Spectra of westward propagating (left) and eastward propagating (right) 30 mb heights in the 120 day control run at 19.4°S. The axis labels have the same meaning as in Fig. 3.

particular wavenumber one mode should be preferentially excited remains puzzling. In the model run used to produce Fig. 4, the radiation calculations were performed ever 3 h and the model-generated fields were saved every 6 h. The same peak was found in spectra computed from the results of simulations with radiation calculations performed at 2.5-h intervals and with fields saved every 18 h. All other aspects involved in the numerical integration of the model (e.g., convective adjustment) are performed every time step (i.e., at 30-min intervals). Thus it seems clear that the 2.4-day wave (and the 4.8-day wave) are not directly excited by artificial periodic aspects of the GCM time-marching scheme.

It would be very interesting to see if other GCMs display similar spurious modes. Various versions of the GFDL grid point model (e.g., Hunt and Manabe (1968)) have produced simulations contaminated by a prominent zonally-symmetric oscillation of about 11.5 hour period (corresponding to the gravest symmetric $s = 0$ external gravity mode). No explanation for the prominence of this particular oscillation in the GFDL model has been advanced.

Fig. 5 displays the spectra of eastward and westward propagating zonal wavenumber two variance of the 250 mb geopotential heights in the GCM at selected latitudes. This figure can be compared with the observational results shown in Fig. 6 of SM (but remembering that the model spectra should be multiplied by 1.25 to make the comparison). It is clear that the overall variance in both westward and eastward propagating $s = 2$ waves is somewhat underestimated in the model at all latitudes (by about a factor of two at 60° N, less seriously at lower latitudes). The model spectra also appear to be redder than the observed spectra (although this problem is less pronounced for $s = 2$ than for $s = 1$). There are peaks in the spectra of westward propagating variance at all latitudes located between about 0.21 and 0.28 day^{-1} (periods between about 3.6 and 4.8 days). These peaks can be tentatively identified with the (2,1) Rossby normal mode or "4-day wave". Also evident, at least at 36° N and 36° S, is a peak between about 0.1 and 0.15 day^{-1} (6.67 to 10.0 days). This is roughly the period range anticipated for the gravest antisymmetric Rossby mode (2,2).

At still lower frequencies, SM's observed spectra of westward propagating wavenumber two variance display peaks near about 20-day period, which might be identified with the (2,3) mode. By contrast, in the model spectra shown in the present Fig. 5a no such peak can be identified.

4.2. Structure of filtered fields

In order to confirm the tentative identification of the peaks seen in the space-time spectra with actual normal modes, a more detailed examination was made of the structure of the zonal wavenumber one and two variance in the model. The approach taken was to resynthesize the geopotentials associated with the westward propagating variance of a particular zonal wavenumber within some fairly narrow frequency interval near the frequencies predicted for the Rossby modes. The resynthesized fields are functions of latitude, longitude, pressure and time, but since only westward propagating components with a particular zonal wavenumber are included, all the information is actually contained in the geopotentials along any individual meridian of longitude.

Fig. 6a shows the reconstructed zonal wavenumber one geopotential height at 36° N in the period range 4.44 to 6.32 days for 40 days during the control run. This and succeeding figures have been plotted with the seven reference levels equally spaced on the pressure axis (resulting in a vertical coordinate that is roughly proportional to height) and the contours have been drawn by hand. At each level in Fig. 6a, there is an oscillation between negative and positive height anomalies with period roughly 5 days. This is guaranteed by the filtering procedure. What is striking, however, is the tendency for these oscillations to be in phase at all levels, i.e., for the wave selected by the filter to have an equivalent barotropic structure. The amplitude of the geopotential oscillation in Fig. 6a obviously undergoes some substantial long period changes. The equivalent barotropic structure of the oscillation is clearest when the amplitude is large; when the amplitude is relatively weak there is some substantial westward phase tilt with height (e.g., around days 32–40 in Fig. 6a).

The detailed vertical structure of the oscillation in Fig. 6a does resemble that of the idealized external mode shown in Fig. 2, particularly when

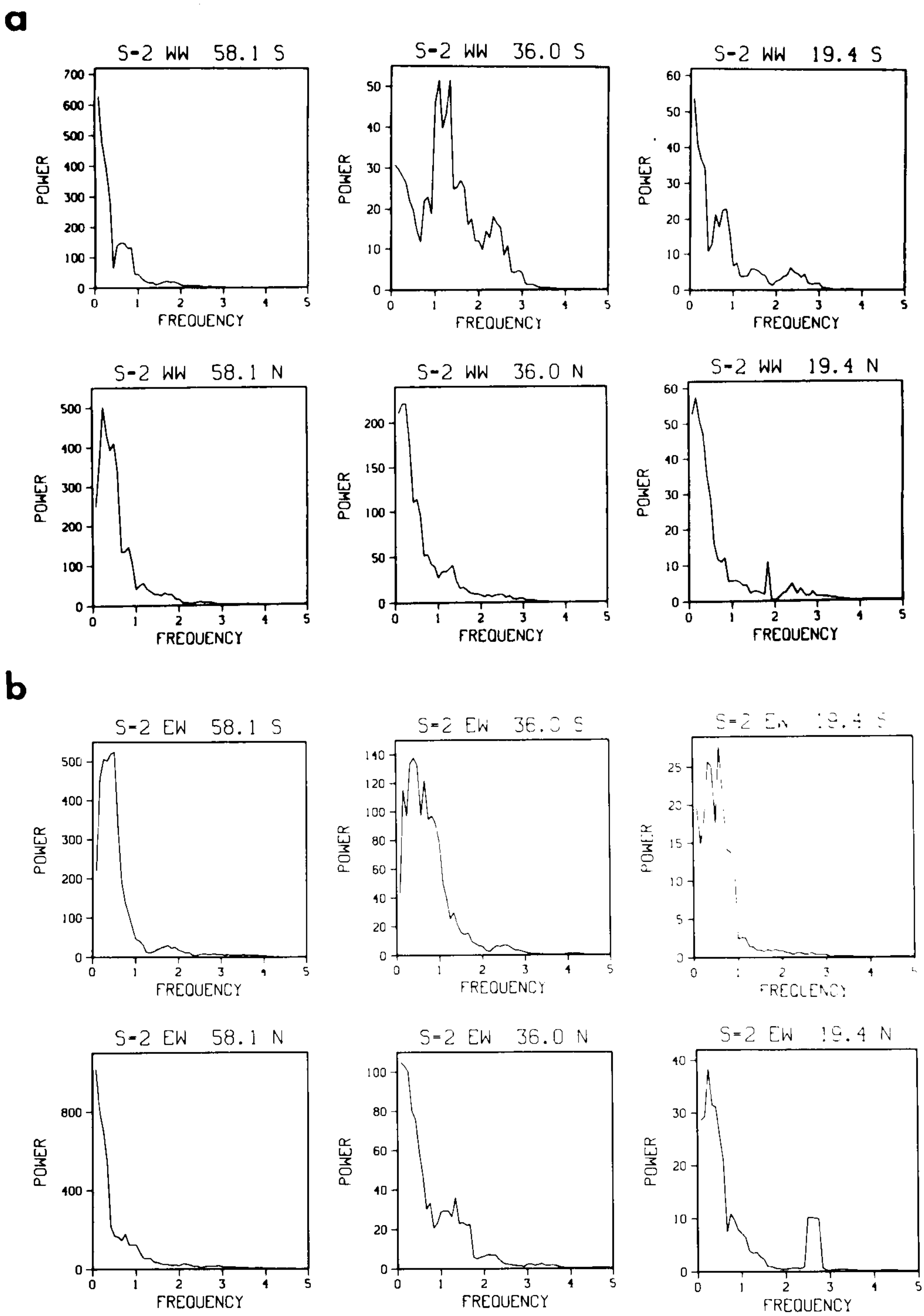

Fig. 5. (a) Spectra of westward propagating zonal wavenumber two variance of the 250 mb height field in the 120-day control run at six selected latitudes. Axis labelling as in Fig. 3. (b) As in (a), but for eastward propagating variance.

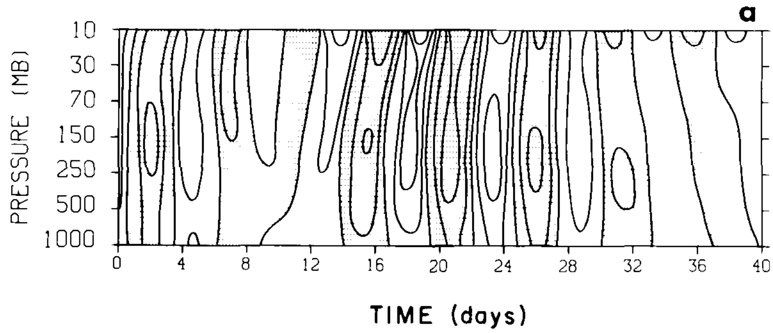

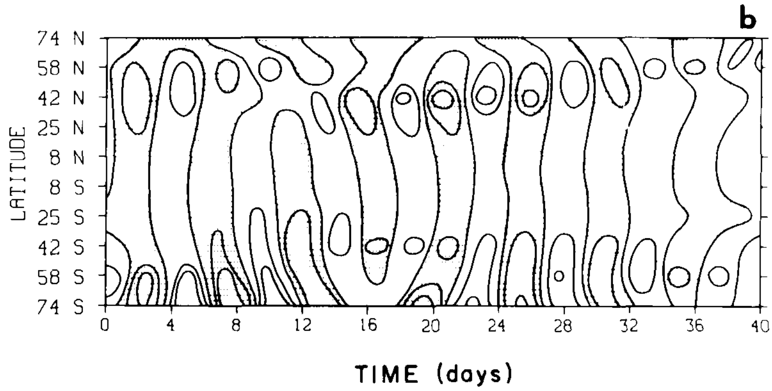

Fig. 6. (a) Time-height section of the geopotential heights at the Greenwich meridian and 36° N during 40 days of the control run. Filtering has been applied to select only westward propagating zonal wavenumber one variance with periods between 4.44 and 6.32 days. Negative anomalies are shaded and the contour interval is 10 m. (b) as in (a), but a time-latitude section of the filtered 250 mb height. The latitudes marked 8, 25, 42, 58 and 74 degrees actually correspond to 8.3, 24.9, 41.5, 58.1 and 74.7 degrees (these are points on the Gaussian grid appropriate for a triangular 20 spectral model).

the wave amplitude is strong. The amplitude of the oscillation in Fig. 6a tends to grow slowly with height, with some extra intensification at the top level. However, in contrast to the idealized modal structure, the simulated geopotential variations in Fig. 6a do sometimes display a local amplitude maximum near the tropopause. Such differences in detail might be attributable to the effects of mean winds and dissipation in distorting the idealized modal structure. In any event, the filtered fields are remarkably like those anticipated for an atmospheric normal mode.

Fig. 6b shows the time-latitude section of the reconstructed 250 mb heights when the same filtering was applied. In this and subsequent figures the reconstructed fields are plotted only to 74.7 degrees latitude. At higher latitudes the behaviour of the filtered fields tends to be rather uncorrelated with the results at lower latitudes. Of course, the rationale for resolving motions into zonally-propagating waves breaks down near the poles.

The filtered fields in Fig. 6b reveal a modal structure (i.e. with the oscillations occurring in phase at all latitudes). The modal nature of the oscillation is clearest where the wave amplitude is strongest; when the wave amplitude is relatively weak some significant meridional phase propagation is apparent (e.g., days 32–40 in Fig. 6b). The geopotential oscillations in this figure have minimum amplitude in the tropics and a relative maximum in the midlatitudes of the northern hemisphere. The behaviour in the southern hemisphere is more complicated; sometimes there is a midlatitude maximum and at other times the amplitude is largest at the highest latitude shown. On the whole, it does seem reasonable to identify the meridional structure of the filtered geopotential with the idealized (1,1) Rossby mode (Fig. 1). Similar horizontal structures are seen when the same filtering is applied to the simulated geopotential at other pressure levels.

The modal structure can be seen in other fields produced by the GCM as well. Figs. 7a and 7b show the reconstructed meridional and zonal winds at 36° N when the same "5-day" wave filter is applied. The roughly equivalent barotropic nature of the oscillation is apparent, particularly when the wave amplitude is strong. It is also noteworthy that the filtered meridional and zonal wind oscillations are roughly a quarter-cycle out of phase throughout most of the simulation. This is also consistent with the expected behaviour of an atmospheric normal mode.

Fig. 8a and 8b present time-height and time latitude sections of the geopotential after filtering designed to pick out the (2,1) Rossby mode ("4-day" wave). The time-height section of the filtered geopotential at 36° N shows an equivalent barotropic structure resembling that of a classical normal mode. The filtered 250 mb heights shown in Fig. 8b reveal a meridional structure clearly identifiable with that of the idealized (2,1) mode.

The gravest antisymmetric modes can also be detected in appropriately filtered time series of the geopotential. While a disturbance resembling the (1,2) mode can be isolated by filtering, the results are more dramatic for the (2,2) mode. Fig. 9 shows the time-height and time-latitude sections of the $s = 2$ geopotential heights filtered between periods of 6.67 and 10.0 days. This period range corresponds to the spectral peaks identified with the (2,2) mode in Fig. 5a. Both the equivalent barotropic vertical structure and the antisymmetric meridional modal structure are clearly revealed in these filtered fields. The typical amplitude of the oscillation shown in Fig.

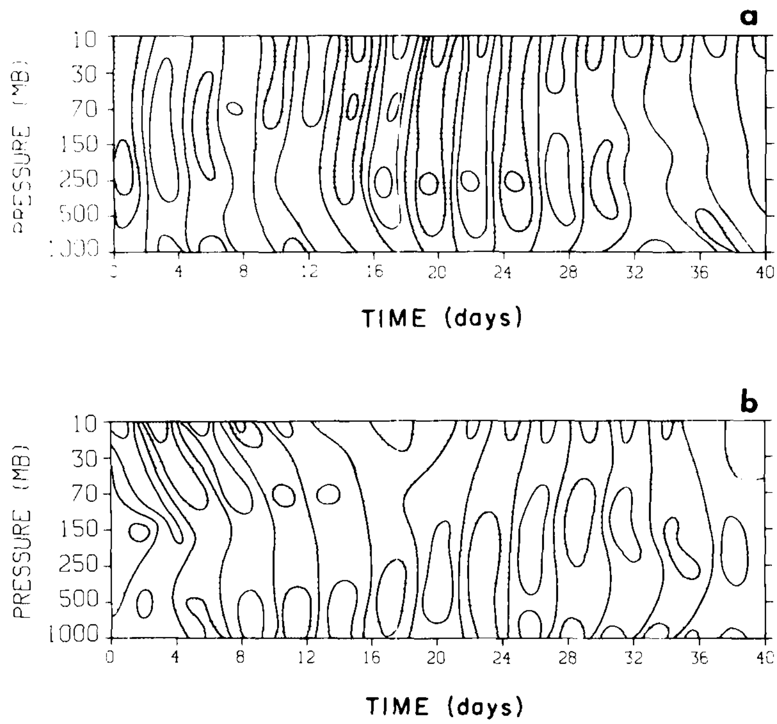

Fig. 7. (a) As in Fig. 6a but for the meridional wind. The contour interval is 0.25 m/s. (b) As in (a), but for the zonal wind. The contour interval is 0.5 m/s.

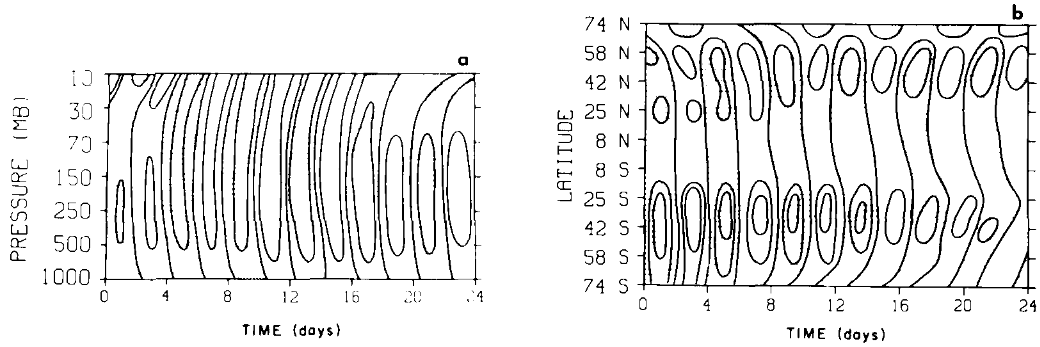

Fig. 8. (a) Time-height section of the geopotential heights at the Greenwich meridian and 36° N during 24 days of the control run. Filtering has been applied to select only westward propagating zonal wavenumber two variance with periods between 3.75 and 4.62 days. The contour interval is 5 m. (b) As in (a), but a time-latitude section of the filtered 250 mb heights.

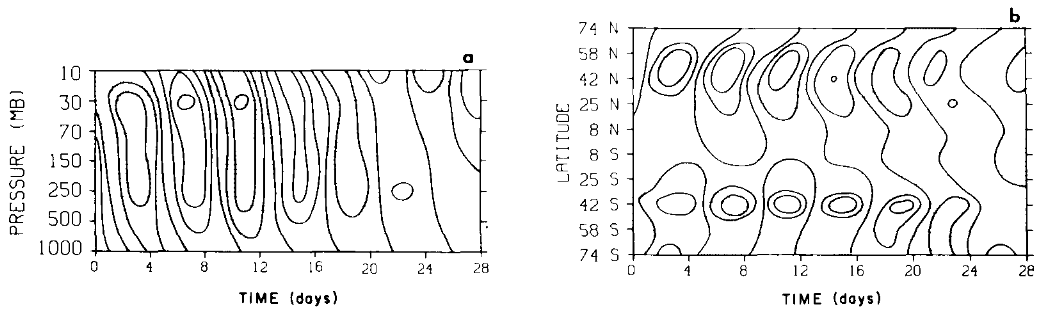

Fig. 9. (a) Time-height section of the geopotential heights at the Greenwich meridian and 36° N during 28 days of the control run. Filtering has been applied to select only westward propagating zonal wavenumber two variance with periods between 6.67 and 10 days. The contour interval is 10 m. (b) As in (a), but a time-latitude section of the filtered 250 mb heights.

9 is about twice that of the gravest symmetric modes shown in Figs. 7 and 8. This is consistent with observations (e.g., Ahlquist, 1985).

As noted earlier, the space-time spectra of the simulated geopotentials do not seem to display isolated peaks identifiable with the (1,3) mode or "16-day" wave, except possibly in the stratosphere. Nonetheless, it is of interest to examine the structure of the variations seen in the appropriate period range in the GCM simulation. Fig. 10 shows the time-height and time-latitude sections of westward propagating wavenumber one geopotential heights in the period range from 12 to 30 days. The time-height section in Fig. 10a is plotted for 58.1° N near where the amplitude of the (1,3) mode is expected to be maximum. The vertical structure of the filtered geopotential in Fig. 10a is roughly equivalent barotropic, but it displays much more intensification in the stratosphere than does the idealized modal structure of Fig. 2. The time-latitude section in Fig. 10b is quite interesting. While there are some rather irregular variations in this filtered time series, there is at least one brief episode when it seems possible to identify patterns that have some resemblence to the idealized (1,3) mode. Note in particular the period between days 48 and 70. During the time between about days 48 and 60, there are negative values in the high latitudes of both hemispheres and small positive values at

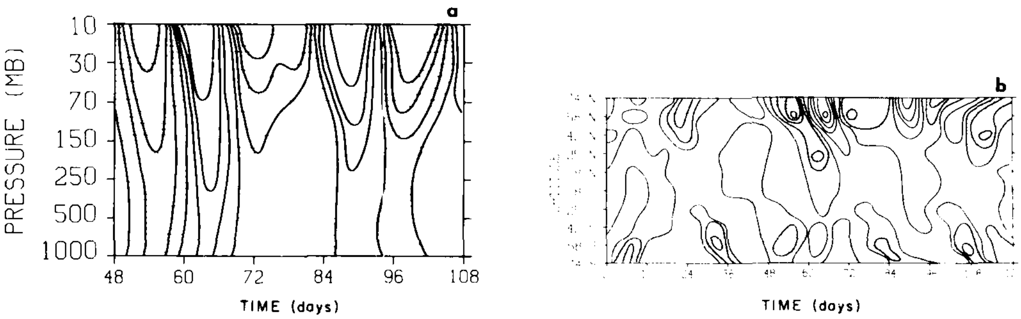

Fig. 10. (a) Time-height section of the geopotential heights at the Greenwich meridian and 58.1° N during 60 days of the control run. Filtering has been applied to select only westward propagating zonal wavenumber one variance with periods between 12 and 30 days. Contours at 50, 100 and 200 m. (b) As in (a), but a time-latitude section of the 250 mb heights for the entire 120-day simulation analyzed. The contour interval is 25 m.

lower latitudes. Then this pattern reverses for about the next ten days, with positive values at high latitudes and small negative values in between. This pattern does resemble that of the classical (1,3) mode. However, very large distortions in the idealized modal structure are clearly present in the model simulation. In particular the signal in the northern (i.e. winter) hemisphere is much larger than that in the southern hemisphere. As noted in Subsection 2.2, a similar kind of asymmetry has been observed in the "16-day" wave in boreal winter (Daley and Williamson, 1985). Finally, it is worth emphasising again that even this very distorted version of the (1,3) mode structure is apparent for only a short fraction of the whole 120-day record.

In addition to the spectral peaks identifiable with the Rossby modes, there are also peaks in stratospheric $s = 1$ spectra at eastward propagating periods of about 2.4 and 4.8 days (see Subsection 4.1 above). The $s = 1$ component of the 30 mb geopotential filtered between periods of 4.0 and 5.22 days is shown in Fig. 11. This oscillation displays a meridional structure that is equatorially trapped, like that anticipated for a Kelvin mode (although there are some large amplitudes at very high latitudes in the northern hemisphere as well). The external Kelvin normal mode in the atmosphere is predicted to have a period of about 33 h (Matsuno, 1980; Hamilton, 1984; Hamilton and Garcia, 1986), and so cannot be identified with the 4.8-day spectral peak seen in the model results. Both the relatively long

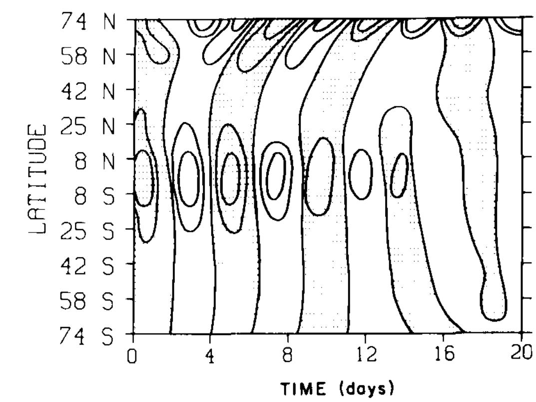

Fig. 11. Time-latitude section of the 10 mb heights along the Greenwich meridian during 20 days of the control run. Filtering has been applied to select only eastward propagating zonal wavenumber one variance with periods between 4.0 and 5.22 days. The contour interval is 5 m.

period and short meridional trapping scale seen in Fig. 11 would be consistent with an identification with an internal Kelvin mode. The internal structure of this disturbance is not really evident in filtered time-height sections (not shown), but the vertical structure in the troposphere may be masked by the large eastward propagating variance in other types of motions at these frequencies. As noted earlier, the scales associated with this oscillation are similar to those observed for prominent internal Kelvin waves in the atmosphere (e.g., Hirota, 1978).

4.3. Time series of mode amplitudes and phases

The filtered time-height and time-latitude sections presented in the previous section all reveal fairly regular oscillations that display a slow amplitude modulation. In the filtered time series, the amplitude variation is constrained to occur on time scales no shorter than the inverse of the filtering bandwidth employed. Another approach to studying the day-to-day evolution of the amplitude of the modes was suggested by the observational work of Eliasen and Machenhauer (1965, 1969) and Lindzen et al. (1984; hereafter LSK).

Following LSK, the time series of 500 mb heights and horizontal wind fields in the 120 day control simulation were "minimally filtered" by removing all eastward propagating Fourier components (but retaining westward propagating waves of all frequencies). Then these fields at each 6-h save interval were resolved into the appropriate classical structures for the (1,1), (1,2), (2,1), and (2,2) Rossby modes appropriate for a 9.36 km equivalent depth atmosphere. This resulted in 120-day time series of amplitudes and phases for each of these modes.

The results for the $s = 1$ and $s = 2$ modes during the first 60 days are shown in Figs. 12 and 13 (the last 60 days are quite similar). These diagrams can be directly compared with the corresponding observations presented in LSK (note that LSK use a different notation to label individual modes). The phases obtained in this kind of analysis tend to be rather irregular when the modal amplitudes are small. Thus, following LSK, the phases in Figs. 12 and 13 are not plotted when the amplitudes fall below 0.2 of their maximum value. The dashed lines in the top parts of each of Figs. 12a, 12b, 13a and 13b show the phase propagation for the modes predicted by the classical theory with a 9.36 km equivalent depth.

The results in Figs. 12 and 13 display the fairly regular westward phase propagation and the significant irregular amplitude variations that have appeared in the earlier observational studies of Eliasen and Machenhauer (1965, 1969) and LSK. The amplitude variations typically take place on time scales of the order of the wave period and the amplitudes range over about an order of magnitude. The amplitude ranges seen in the present GCM results are quite comparable to those presented in the observations of LSK.

Table 2 compares the maximum amplitudes obtained in the present analysis of model results with the observational values quoted by LSK. It

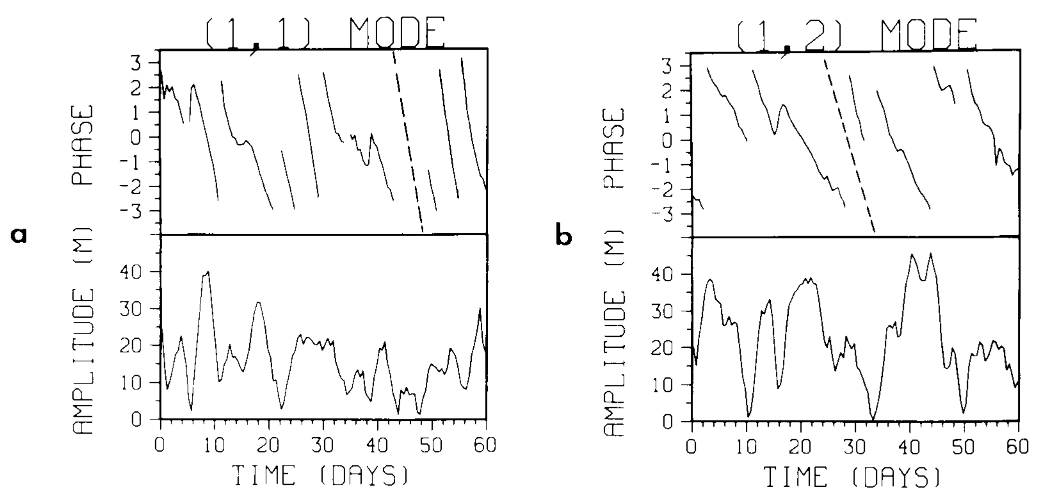

Fig. 12. Amplitude (in term of geopotential) and phase of the projection of the 500 mb geopotential height and horizontal wind onto the classical (1,1) Rossby mode during the first 60 days of the control run. The phases are not plotted when the amplitude drops below 20% of its maximum value. The dashed line shows the phase propagation predicted for the (1,1) mode in the classical theory. (b) As in (a), but for the (1,2) mode.

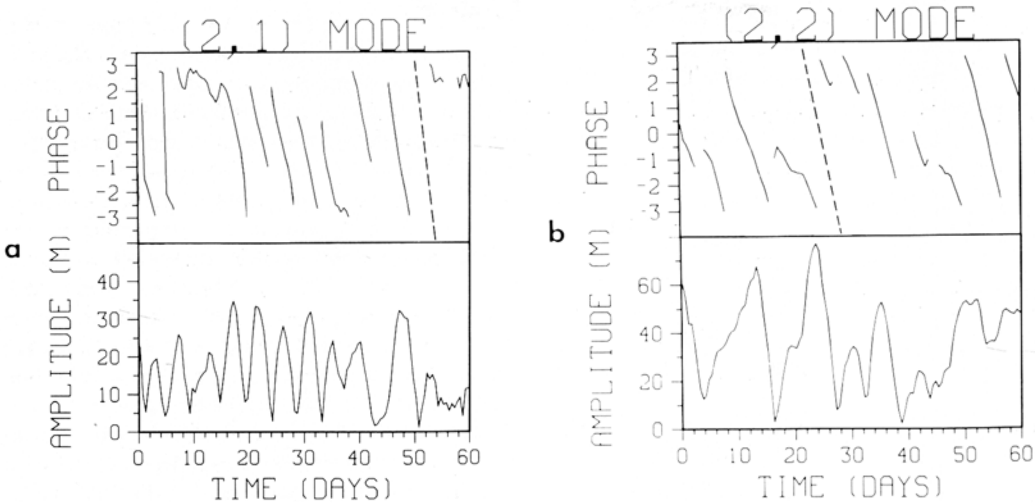

Fig. 13. (a) As in Fig. 12, but for the (2,1) mode. (b) As in Fig. 12, but for the (2,2) mode.

Table 2. *Maximum 500 mb height amplitudes obtained for the classical modes of Fig. 1 in the 120-day segment of the control run of the GCM, compared with the maxima found by Lindzen et al. (1984) in a year of observations; the final column gives the root-mean-square values of the modal amplitudes in the simulation; all values in metres and multiply the dimensionless eigenfunctions shown in Fig. 1*

Mode	Present maximum	Lindzen et al.	RMS
(1,1)	42.4	34	18.0
(1,2)	48.1	65	25.7
(1,3)	80.1	76	37.2
(2,1)	55.6	40	18.6
(2,2)	79.5	65	33.5
(2,3)	79.8	74	47.8

should be noted that the present GCM results are for a 120-day period, while LSK's values represent the maxima observed during an entire year. The maximum amplitudes in the simulation are quite comparable to those from the observations. Also quoted in Table 2 are the root mean square amplitudes of the Rossby modes during the 120-day segment analyzed. These values are in rough agreement with the observed mean amplitudes obtained by Ahlquist (1985).

5. Comparison of results in control and El Niño simulations

Hamilton (1985) examined the strength of the spectral signal associated with the (1,1) Rossby mode observed in northern hemisphere sea level pressure data in a series of 17 individual years. He then demonstrated a statistically significant correlation between the strength of the (1,1) mode and the sea surface temperature averaged over a large region of the tropical Pacific Ocean. In particular the observations suggest that the five day wave tends to be stronger (weaker) in the warm (cold) phase of the Southern Oscillation. As noted in Section 3, the Canadian Climate Centre GCM has been run through a 10-year control simulation and through a number of winter simulations with enhanced SSTs in the tropical Pacific. The history tapes from these model experiments were employed to study the effect of El Niño conditions on the strength of the simulated (1,1) Rossby mode.

The geopotential fields in the 78.75 day segments from each of the ten control winters and five El Niño experiments were subjected to space-time spectral analysis in a manner similar to that described in Section 4. The (1,1) mode was then isolated by resynthesizing the geopotential variations associated with westward propagating zonal wavenumber one with periods between 4.375 and 6.057 days. Then an estimate of the global amplitude of the mode was made as follows. First, at each save time the quantity v was computed as

$$v = \int_{-\pi/2}^{\pi/2} \phi' \cos \theta \, d\theta$$

where θ is the latitude and ϕ' is the filtered geopotential at the Greenwich meridian. The geopotential amplitude for the mode was then taken to be the r.m.s. value of v throughout the entire 78.75-day interval. A height amplitude was then obtained by dividing this geopotential amplitude by g.

Fig. 14 shows the height amplitudes computed at the 1000, 500 and 250 mb levels in each of the 15 cases. There is an obvious tendency for the amplitude to be larger in the El Niño simulations than in the control simulation. The differences in the mean values of the amplitudes in the ten control winters and those in the five El Niño winters is statistically significant at the 95% confidence level at both 1000 mb and 250 mb, when judged with a standard t-test.

The interpretation of the connection between tropical SSTs and the (1,1) Rossby mode seen in both observations and in the GCM simulation is complicated by the fact that the SST variability is related to changes in many aspects of the global scale circulation (e.g., Horel and Wallace, 1981). However, the most direct atmospheric effect would appear to relate to the geographical distribution of latent heat release. In particular, there is a strong eastward shift of the precipitation observed in the tropical Pacific region during the mature phase of El Niño events (e.g., Rasmusson and Carpenter, 1982). This change in precipitation is well simulated by the Canadian Climate Centre GCM (Boer, 1985). Hamilton (1985) suggested that the most reasonable interpretation of his observational results would involve the supposition that latent heat release represents a major excitation for the (1,1) mode. The observed interannual variations in the strength of the 5-day wave would then be related to the modulation of this forcing by the Southern Oscillation.

It is interesting to note that Tokioka et al. (1985) have performed a controlled experiment with the Japanese Meteorological Research Institute GCM in which they added a warm SST anomaly in the tropical Pacific during boreal summer. They found an enhanced 5-day wave in the experiment with the SST anomaly, in agreement with the present results.

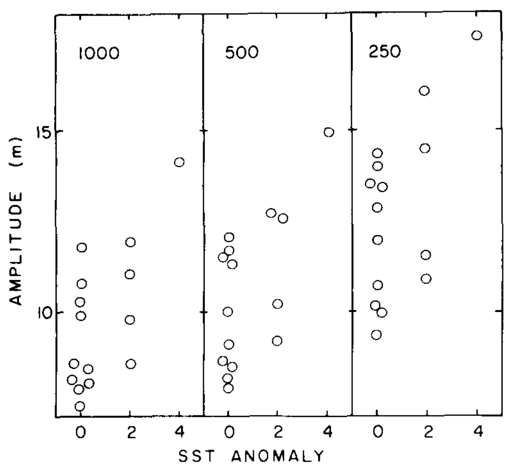

Fig. 14. The geopotential height amplitude of the (1,1) mode determined at the 1000, 500 and 250 mb levels during 10 individual winters of an integration performed with climatological SSTs, 4 winters with 2 × a standard "El Niño" SST anomaly imposed in the tropical Pacific and one winter with 4 × the standard SST anomaly.

6. Energetics of the modes in the model

In the real atmosphere the external Rossby mode amplitudes must be controlled by some balance between forcing and dissipation mechanisms. The diagnosis of the dominant sources of modal excitation and dissipation from real data is a very difficult task. Thus the few comments in the literature relating to the question of forcing and dissipation have been largely speculative. For example, Garcia and Geisler (1981) suggested that varying zonal flow over the earth's large scale topography could act as a significant forcing mechanism for the 5-day wave. Hamilton's (1985) suggestion that latent heat release could be important for the 5-day wave has been noted above. Obvious sources for dissipation are infrared radiative cooling, and boundary layer friction (e.g., Salby, 1980). In addition, the nonlinear dynamical interactions with all other scales of motion can act as either a source or sink for modal energy.

The Canadian Climate Centre GCM has produced an excellent simulation of the amplitudes and structures of the (1,1), (1,2), (2,1) and (2,2) modes and has even captured the observed dependence of the (1,1) mode amplitude on tropical SST. This leads one to hope that the actual balance of forcing and dissipation for these Rossby modes in the GCM may be realistic. As part of the present project, a simple diagnostic calculation of the energetics of the prominent Rossby normal modes was attempted.

The basic premise of this analysis was that the application of a fairly narrow space-time spectral filter can select out motions associated with a particular mode. Table 3 gives the period ranges employed in the filters used to isolate the modes. The period ranges for the (1,1), (2,1) and (2,2) modes given in this table are just those employed to produce the filtered fields shown in Figs. 6–9. The very clean results in these figures lend support to the idea that filtering can isolate variance connected with the individual modes.

The development of the appropriate energy equations is presented in the Appendix. The first step was simply to define the modal energy as the sum of kinetic and available potential energies in the filtered fields (see eq. A5). Then it is straightforward to derive an equation relating the rate of change of the globally integrated modal energy to integrals of correlations of various filtered quantities (eq. A8). The correlation terms written explicitly in eq. (A8) are easy to interpret physically. Thus the correlation of vertical velocity with geopotential along the lower boundary represents the role of mountain torques in generating or dissipating the mode. The correlation of diabatic heating with the vertical derivative of the geopotential is the usual generation term for available potential energy. The correlation of velocities with the subgrid scale momentum forcing might be regarded as a measure of "frictional dissipation". In addition, the energy equation includes contributions derived from the nonlinear advective terms in the momentum and thermodynamic equations. These have a rather complicated form and cannot be resolved simply into the usual categories familiar from simple zonal mean/eddy diagnostics. In the present study no attempt was made to compute these terms.

Table 3. *Period limits for the filters applied to isolate the Rossby modes in the energetics analysis described in Section 6*

Mode	Period limits (days)
(1,1)	4.44–6.32
(1,2)	8.00–15.00
(2,1)	3.75–4.62
(2,2)	6.67–10.00

In the GCM simulation analyzed in the present study, only selected fields generated by the model had been archived. One significant limitation was that the vertical distribution of latent heat release was not saved; only the precipitation rates at each time step were available. Another important problem was that the subgrid scale contributions to the momentum and thermodynamic equations were not saved; only the subgrid scale surface stresses and heat fluxes were available. As shown in the Appendix, the contributions of the subgrid scale terms to the energy balance of the modes can be divided into expressions involving only the surface fluxes and expressions involving only the fluxes in the interior of the atmosphere. When this separation is incorporated into the energy equation, the result is the eq. (A11).

In the present study, the only contribution to the subgrid scale dissipation of energy computed was that involving the surface fluxes. The other "internal" dissipation term will be negative if downgradient subgrid scale fluxes dominate.

The actual evaluation of the terms in eq. (A11) was further simplified by the use of model generated fields that had been interpolated or extrapolated from sigma coordinates onto pressure surfaces from 1000 mb to 10 mb. Thus the surface integrals in terms 1 and 2 of this equation were actually performed over the 1000 mb surface, and the volume integrals extended from 1000 to 10 mb over the entire globe.

The energetics analysis outlined above was applied to the 120-day segment of the control run that has been discussed extensively in Section 4 above. The various terms in eq. (A11) were evaluated at each save time and then mean values of each term for the full 120 days were computed.

Table 4 summarizes the results for each of the four modes considered. Also given in Table 4 is the total energy in each mode averaged over the entire 120-day period.

The largest dissipation term for each of the modes is that due to the subgrid scale fluxes (i.e., term 2 in eq. (A11)). It turns out that the contribution to this term from surface heat fluxes is much smaller than that from surface stresses, and so it may be reasonable to refer to this term as the "surface friction". As noted above, it is likely that the subgrid scale stresses in the interior of the atmosphere will be dominated by downgradient transfers, and so the total effect of all subgrid scale fluxes in the model is probably even more strongly dissipative than indicated by the values given in Table 4 for surface friction alone.

Table 4. *Estimated contributions to the global energy budget of the 2 gravest Rossby modes of zonal wavenumbers one and two, averaged over the 120-day segment of the control run*

Mode	Radiation	Topographic interaction	Friction	Total energy
(1,1)	−31	−12	−1074	704
(1,2)	−813	−229	−4728	2536
(2,1)	−2	−15	−137	322
(2,2)	−161	−175	−2404	1095

The column headed "radiation" gives the estimates of the term 3 in eq. (A11). The "topographic interaction" is the estimate of term 1 in (A11). The "friction" is the estimate of term 2 in (A11). Values for all these quantities are quoted in gigawatts. The final column gives the estimated total energy in each mode (see A5) averaged over the 120-day period. The total energy is given in units of 10^{15} J.

The effects of radiative transfer on the modes is dissipative, but is less important than the frictional terms in this regard. It is interesting (and somewhat surprising) that the radiative dissipation of the (1,1) and (2,1) modes is so much less effective than that for the (1,2) and (2,2) modes.

The topographic interactions act, on average, as net sinks for the energy of each of the modes. It is still possible, however, that the topographic interaction with the overlying flow could act sporadically to excite normal modes in the manner envisaged by Garcia and Geisler (1981). The rather small average effect of topography seen in the present results is consistent with the GCM experiments of Hayashi and Golder (1983). They found little difference in their results for the "16-day" wave in model simulations with and without topography.

A rough estimate of the mean dissipation time scale for the modes can be obtained by dividing the total energy quoted in Table 4 by the sum of the dissipation rates from surface friction, radiation and topographic interaction (since the internal frictional dissipation is not included, this should lead to an overestimate of the time scale). This time scale turns out to be of the order of five to ten days for each of the modes. Rather similar estimates of the dissipation time scale can be obtained from the width of the peaks in the space-time spectra of the model fields shown in Figs. 3a and 5a.

As noted earlier, the vertical distribution of the

Table 5. *Area weighted correlation coefficients between time series of precipitation and the time series of temperature interpolated onto various pressure levels*

Level (mb)	(1,1) mode	(1,2) mode	(2,1) mode	(2,2) mode
970	0.011	0.023	0.019	0.014
880	0.025	0.032	0.017	0.029
750	0.045	0.026	−0.013	0.004
550	0.012	0.021	−0.033	0.015
360	0.054	−0.022	0.008	0.005
235	0.101	−0.047	0.042	−0.060

The space-time filters used to isolate individual modes have been applied before the correlation coefficients were computed. See text for details.

latent heat release was not archived from the GCM run. The correlations between the precipitation (which in the model is exactly proportional to the vertically-integrated heating) and the temperature at various levels is shown in Table 5, for the different space-time filters. The correlations are all rather low (although it should be borne in mind that there are a large number of degrees of freedom that go into the calculation of these coefficients since they represent global averages). There does appear to be a general tendency for the precipitation to correlate positively with the filtered temperatures, presumably indicating a net positive energy source for the modes from latent heat release. If one makes an arbitrary vertical distribution of the total latent heat release (e.g., by assuming a constant heating rate per unit mass from 1000 mb to 350 mb), then term 4 in eq. (A11) can be estimated from the precipitation and temperature data. If this is done then it appears that the latent heat release contribution to the modal energetics is comparable in magnitude to the surface dissipation (term 1). However, it must be emphasized that the results of such an analysis are quite sensitive to the assumed vertical structure of the heating.

Hayashi and Golder (1983b) found that nonlinear wave-wave interactions represented a very important excitation mechanism for westward propagating normal modes in a GFDL GCM. The effects of non-linearities have not been assessed in the present study.

7. Conclusions

Simulations produced by a modern tropospheric/lower stratospheric GCM were examined to detect prominent motions that could be identified as normal mode oscillations. The results provided a clear indication of the presence of the 2 gravest external Rossby modes of both zonal wavenumbers 1 and 2. The presence of these modes was manifested as isolated peaks in the space-time spectra of model generated fields. The detailed vertical and meridional structures of these oscillations were investigated by filtering the simulated geopotential and wind fields in narrow bands around the spectral peaks. The vertical structures of the appropriately filtered fields were approximately equivalent barotropic, and the meridional structures resembled the idealized modes of classical theory (except possibly at high latitudes). The amplitudes of the oscillations evident in the filtered time series undergo strong modulations, but typical amplitudes are in reasonable accord with observations. The day-to-day modulation of the amplitude of the modes was studied further by expanding the 500 mb heights and horizontal winds at each available time into the appropriate classical modes. The resulting time series of amplitude determinations for each mode displayed variations on time scales of the order of the wave period, and ranging over about an order of magnitude. These features of the model simulation are in reasonable agreement with comparable observations published recently by Lindzen et al. (1984).

The analysis of the model results failed to reveal any prominent component of the motion that could be clearly identified with the second gravest symmetric Rossby mode of wavenumber one (the "16-day" wave). At least during some brief periods, however, the low frequency westward propagating variance in the model simulation does resemble the idealized (1,3) Rossby normal mode, but distorted to have much larger amplitudes in the winter hemisphere than in the summer hemisphere.

The present analysis revealed evidence for the existence of other prominent, coherent modal structures in the GCM simulation that could not be identified with external normal modes. It is not clear that these oscillations have any counterpart in the real atmosphere and they may owe their appearance in the simulation to the unrealistic upper boundary condition employed in the GCM.

A simple diagnostic analysis of the energetics of the 2 gravest Rossby modes of $s = 1$ and $s = 2$ was conducted. The major dissipation mechanism for the modes appears to be the parameterized friction in the model. Topographic interactions and radiative transfer also act as sources of dissipation for the modes. It is possible that nonlinear dynamical interactions may play an important role in maintaining the modes in the GCM, as suggested by Hayashi and Golder (1983b), but this issue was not investigated in the present project.

8. Acknowledgments

The author is grateful to George Boer for his invitation to visit and use the facilities at the Canadian Climate Centre, and for his interest throughout the project. Many staff members at the Climate Centre provided assistance and suggestions during this work. Particular thanks are due to Mike Lazare for his help. The comments of two anonymous reviewers helped improve the manuscript. This investigation was supported in part by the Canadian Natural Sciences and Engineering Research Council. Many of the numerical calculations were performed on the Canadian Atmospheric Environment Service Cray-1 computer.

9. Appendix. Filtered energy equations

If the prime operator denotes the Fourier filter that selects the westward propagating disturbances of a particular zonal wavenumber within some frequency range, the filtered primitive equations in log-pressure coordinates (e.g., Holton, 1975) can be written

$$\frac{\partial u'}{\partial t} - fv' + \frac{1}{a\cos\theta}\frac{\partial \phi'}{\partial \lambda} - F_x' = NLT, \tag{A1}$$

$$\frac{\partial v'}{\partial t} + fu' + \frac{1}{a}\frac{\partial \phi'}{\partial \theta} - F_y' = NLT, \tag{A2}$$

$$\frac{\partial \phi_z'}{\partial t} + N^2 w' - Q' - \mathscr{H}' = NLT, \tag{A3}$$

$$\frac{1}{a\cos\theta}\frac{\partial u'}{\partial \lambda} + \frac{1}{a\cos\theta}\frac{\partial}{\partial\theta}(v'\cos\theta) + \frac{1}{\rho_0}\frac{\partial}{\partial z}(\rho_0 w') = 0, \tag{A4}$$

where θ and λ are the latitude and longitude, u, v are the usual horizontal wind components, N is the Brunt-Väisälä frequency as defined in Holton (1975), ϕ is the geopotential, F_x and F_y are convergences of the Reynolds' stresses in the northward and eastward directions associated with unresolved motions, $\mathscr{H}$ is proportional to the convergence of the temperature flux associated with the unresolved motions, Q is proportional to the diabatic heating rate, z is proportional to the logarithm of pressure, ρ_0 is equal to $\exp(-z/H)$ where H is a mean scale height. The terms F_x, F_y and $\mathscr{H}$ are parameterized in the model in terms of the resolved variables (Boer et al., 1984a). The "NLT" in eqs. (A1)–(A3) represents the resolved nonlinear advective terms. If the energy/unit mass in the mode of interest is defined as

$$E = \frac{1}{2}\left((u')^2 + (v')^2 + \left(\frac{\phi_z'}{N}\right)^2\right). \tag{A5}$$

It is easy to show from (A1)–(A3) that E is governed by

$$\frac{\partial E}{\partial t} = \frac{-u'}{a\cos\theta}\frac{\partial\phi'}{\partial\lambda} - \frac{v'}{a}\frac{\partial\phi'}{\partial\theta} - w'\phi_z' + u'F_x' + v'F_y' + \frac{\mathscr{H}'\phi_z'}{N^2} + \frac{Q'\phi_z'}{N_2}. \tag{A6}$$

Or, using the continuity equation

$$\frac{\partial E}{\partial t} = -\frac{1}{a\cos\theta}\frac{\partial}{\partial\lambda}(u'\phi') - \frac{1}{a\cos\theta}\frac{\partial}{\partial\theta}(v'\phi'\cos\theta) - \frac{1}{\rho_0}\frac{\partial}{\partial z}(\rho_0 w'\phi') + u'F_x' + v'F_y' + \frac{\mathscr{H}'\phi_z'}{N^2} + \frac{Q'\phi_z'}{N^2} + NLT. \tag{A7}$$

Integrating over the entire model domain one obtains

$$\frac{\partial}{\partial t}\iiint \rho_0 E\,\mathrm{d}V = \iint_{\text{surface}} \rho_0 w'\phi'\,\mathrm{d}A - \iint_{\text{top}} \rho_0 w'\phi'\,\mathrm{d}A + \iiint \rho_0 \frac{Q'\phi_z'}{N^2}\,\mathrm{d}V + \iiint \rho_0\left(u'F_x' + v'F_y' + \frac{\mathscr{H}'\phi_z'}{N^2}\right)\mathrm{d}V \tag{A8}$$

where "surface" and "top" refer to the earth's surface and the top level of the model, respectively. For such large scale waves as the normal modes considered here, the effects of horizontal eddy transports on the unresolved scales are presumably small. The effects of the vertical transports can be written as the sum of surface terms and internal terms. For example, the subgrid scale forcing of the zonal momentum equation can be written as

$$F_x = \frac{1}{\rho_0}\frac{\partial\tau_{xz}}{\partial z}, \tag{A9}$$

where τ_{xz} is the appropriate component of the Reynold's stress tensor. So

$$\iiint \rho_0 F_x' u' \,\mathrm{d}V = \iint \mathrm{d}A \int u' \frac{\partial \tau_{xz}}{\partial z}$$
$$= \underbrace{\iint_{\text{top}} u'\tau_{xz}' \,\mathrm{d}A}_{1} - \underbrace{\iint_{\text{surface}} u'\tau_{xz}' \,\mathrm{d}A}_{2}$$
$$- \underbrace{\iiint \tau_{xz}' \frac{\partial u'}{\partial z} \,\mathrm{d}V}_{3}. \tag{A10}$$

The stress at the top level (and hence term 1) are presumably negligible. If the subgrid scale vertical transfers in the model are dominated by downgradient fluxes, then term 3 is guaranteed to be negative. For the rather barotropic structures that are selected by the space-time filters (particularly those for the (1,1), (1,2), (2,1), and (2,2) modes; see Subsection 4.2) the "surface" term 2 may be an important fraction of the entire mechanical dissipation. Similar manipulations can be applied to terms involving the subgrid scale terms in the meridional momentum and thermodynamic equations. Using these results and separating Q' into radiative and latent heating components, Q_{ra}' and Q_{lh}' one obtains

$$\frac{\partial}{\partial t} \iiint \rho_0 E \,\mathrm{d}V = \underbrace{\iint_{\text{surface}} \rho_0 w'\phi' \,\mathrm{d}A}_{1}$$
$$+ \underbrace{\iint_{\text{surface}} (u'\tau_{xz}' + v'\tau_{yz}' + \phi_z' \eta') \,\mathrm{d}A}_{2}$$
$$+ \underbrace{\iiint \rho_0 \frac{Q_{\mathrm{ra}}' \phi_z'}{N^2} \,\mathrm{d}V}_{3} + \underbrace{\iiint \rho_0 \frac{Q_{\mathrm{lh}}' \phi_z' \,\mathrm{d}V}{N^2}}_{4}$$
$$+ \text{"internal dissipation"} + NLT, \tag{A11}$$

where η is proportional to the subgrid scale vertical temperature flux. Term 1 is the topographic interaction, term 2 represents the "surface" dissipation, terms 3 and 4 are the forcing or dissipation associated with radiation and latent heating. The "surface" dissipation term should include most of the dissipation associated with the surface boundary layer in the model, but will also include some of the effects of the subgrid scale gravity wave drag parameterization, which may actually be dissipating the energy of normal modes in the upper troposphere or stratosphere of the model. The pressure work term at the top level has been ignored in eq. (A11).

REFERENCES

Ahlquist, J. E. 1985. Climatology of normal mode Rossby waves. *J. Atmos. Sci. 42*, 2059–2068.

Boer, G. J., McFarlane, N. A., Laprise, R., Henderson, J. D. and Blanchet, J.-P. 1984a. The Canadian Climate Centre spectral atmospheric general circulation model. *Atmosphere-Ocean 22*, 397–429.

Boer, G. J., McFarlane, N. A. and Laprise, R. 1984b. The climatology of the Canadian Climate Centre general circulation model as obtained from a five year simulation. *Atmosphere-Ocean 22*, 430–473.

Boer, G. J. 1985. Modelling the atmospheric response to the 1982/83 El Nino. *Coupled Ocean-Atmosphere Models* (J. C. J. Nihoul, ed.), Elsevier, Amsterdam, 7–17.

Daley, R., Tribbia, J. and Williamson, D. L. 1981. The excitation of large-scale free Rossby waves in numerical weather prediction. *Mon. Wea. Rev. 109*, 1836–1861.

Daley, R. and Williamson, D. L. 1985. The existence of free Rossby waves during January 1979. *J. Atmos. Sci. 42*, 2121–2141.

Desmarais, J. G. and Derome, J. 1978. Some effects of vertical resolution on modelling forced planetary waves with a time-dependent model. *Atmosphere-Ocean 16*, 212–225.

Dikii, L. 1965. The terrestrial atmosphere as an oscillating system. *Izv. Acad. Sci. USSR Atmos. Oceanic Phys.*, Engl. trans., *1*, 469–489.

Dikki, L. and Golitsyn, G. 1968. Calculation of Rossby wave velocities of the earth's atmosphere. *Tellus 20*, 314–317.

Eliasen, E. and Machenhauer, B. 1965. A study of the fluctuations of atmospheric planetary flow patterns represented by spherical harmonics. *Tellus 17*, 220–238.

Eliasen, E. and Machenhauer, B. 1969. On the observed large-scale atmospheric wave motions. *Tellus 21*, 149–165.

Garcia, R. R. and Geisler, J. E. 1981. Stochastic forcing of small amplitude oscillations in the stratosphere. *J. Atmos. Sci. 38*, 2187–2197.

Geisler, J. and Dickinson, R. E. 1976. The five-day wave on the sphere with realistic zonal winds. *J. Atmos. Sci. 33*, 632–641.

Hamilton, K. 1984. Evidence for a normal mode Kelvin wave in the atmosphere. *J. Meteorol. Soc. Japan 62*, 308–311.

Hamilton, K. 1985. A possible relationship between tropical ocean temperatures and the observed amplitude of the atmospheric (1,1) Rossby normal mode. *J. Geophys. Res. 90*, 8071–8074.

Hamilton, K. and Garcia, R. R. 1986. Theory and observations of short period atmospheric normal modes. *J. Geophys. Res. 91*, 11867–11875.

Haurwitz, B. 1940. The motion of atmospheric disturbances on the spherical earth. *J. Mar. Res. 3*, 244–267.

Hayashi, Y. 1971. A generalized method of resolving disturbances into progressive and retrogressive waves by space Fourier and time cross-spectral analysis. *J. Meteorol. Soc. Japan 49*, 125–128.

Hayashi, Y. 1974. Spectral analysis of tropical disturbances appearing in a GFDL general circulation model. *J. Atmos. Sci. 31*, 180–218.

Hayashi, Y. and Golder, D. G. 1983a. Transient planetary waves simulated by GFDL spectral general circulation models. I. Effects of mountains. *J. Atmos. Sci. 40*, 941–950.

Hayashi, Y. and Golder, D. G. 1983b. Transient planetary waves simulated by GFDL spectral general circulation models. II. Effects of nonlinear energy transfer. *J. Atmos. Sci. 40*, 951–957.

Hirota, I. 1978. Equatorial waves in the upper stratosphere and mesosphere in relation to the semiannual oscillation of the zonal wind. *J. Atmos. Sci. 35*, 714–722.

Hirota, I. and Hirooka, T. 1984. Normal mode Rossby waves observed in the upper stratosphere. Part I: First symmetric modes of zonal wavenumbers one and two. *J. Atmos. Sci. 41*, 1253–1267.

Hirota, I. and Hirooka, T. 1985. Normal mode Rossby waves observed in the upper stratosphere. II. Second antisymmetric and symmetric modes of zonal wavenumbers one and two. *J. Atmos. Sci. 42*, 536–548.

Holton, J. R. 1975. *The dynamical meteorology of the stratosphere and mesosphere. Meteor. Monogr. No. 37.* Amer. Meteor. Soc., 216 pp.

Horel, J. D. and Wallace, J. M. 1981. Planetary scale atmospheric phenomena associated with the Southern Oscillation. *Mon. Wea. Rev. 109*, 813–819.

Hunt, B. G. and Manabe, S. 1968. An investigation of the thermal tidal oscillations in the earth's atmosphere using a general circulation model. *Mon. Wea. Rev. 96*, 753–766.

Kasahara, A. 1976. Normal modes of ultralong waves in the atmosphere. *Mon. Wea. Rev. 104*, 669–690.

Lamb, H. 1932. *Hydrodynamics*, 6th edition. Dover, New York, 548–549.

Lambert, S. J. and Merilees, P. E. 1978. A study of planetary wave errors in a spectral numerical weather prediction model. *Atmosphere-Ocean 16*, 197–211.

Lindzen, R. S., Straus, D. M. and Katz, B. 1984. An observational study of large-scale atmospheric Rossby waves during FGGE. *J. Atmos. Sci. 41*, 1320–1335.

Longuett-Higgins, M. S. 1968. The eigenfunctions of Laplace's Tidal Equation over a sphere. *Philos. Trans. R. Soc. London A262*, 511–607.

Madden, R. A. 1978. Further evidence of traveling planetary waves. *J. Atmos. Sci. 35*, 1605–1618.

Madden, R. A. 1979. Observations of large-scale travelling waves. *Rev. Geophys. Space Phys. 17*, 1935–1949.

Madden, R. A. 1983. The effect of the interference of traveling and stationary waves on time variations of the large-scale circulation. *J. Atmos. Sci. 40*, 1110–1125.

Madden, R. A. and Julian, P. 1972. Further evidence of global-scale five-day pressure waves. *J. Atmos. Sci. 29*, 1464–1469.

Madden, R. A. and Julian, P. 1973. Reply to comments of R. Deland. *J. Atmos. Sci. 30*, 935–940.

Matsuno, T. 1980. A trial search for minor components of lunar tides and short-period free oscillations of the atmosphere in surface pressure data. *J. Meteorol. Soc. Japan 58*, 281–285.

Pratt, R. and Wallace, J. M. 1976. Zonal propagation characteristics of large-scale fluctuations in the midlatitude troposphere. *J. Atmos. Sci. 33*, 1184–1194.

Rasmusson, E. M. and Carpenter, T. H. 1982. Variations in tropical sea surface temperature and surface wind fields associated with the Southern Oscillation/El Niño. *Mon. Wea. Rev. 110*, 354–384.

Rodgers, C. D. 1976. Evidence for the five day wave in the upper stratosphere. *J. Atmos. Sci. 33*, 710–711.

Salby, M. L., 1979. On the solution of the homogeneous vertical structure problem. *J. Atmos. Sci. 36*, 2350–2359.

Salby, M. L. 1980. The influence of realistic dissipation on planetary normal structures. *J. Atmos. Sci. 37*, 2186–2199.

Salby, M. L. 1981a. Rossby normal modes in nonuniform background configuration, I, simple fields. *J. Atmos. Sci. 38*, 1803–1826.

Salby, M. L. 1981b. Rossby normal modes in nonuniform background configuration, II, equinox and solstice conditions. *J. Atmos. Sci. 38*, 1827–1840.

Salby, M. L. 1984. Survey of planetary-scale traveling waves: the state of theory and observations. *Rev. Geophys. Space Phys. 22*, 209–236.

Schoeberl, M. R. and Clark, J. H. E. 1980. Resonant planetary waves in a spherical atmosphere. *J. Atmos. Sci. 37*, 20–28.

Speth, P. and Madden, R. A. 1983. Space-time spectral analysis of Northern Hemisphere geopotential heights. *J. Atmos. Sci. 40*, 1086–1100.

Tokioka, T., Yamazaki, Y. and Chiba, M 1985. Atmospheric response to the sea surface temperatures observed in early summer 1983—a numerical experiment. *J. Meteorol. Soc. Japan 63*, 565–588.

Tsay, C. 1974. Analysis of large-scale wave disturbances in the tropics simulated by an NCAR general circulation model. *J. Atmos. Sci. 31*, 330–339.

Williamson, D. L. and Dickinson, R. E. 1976. Free oscillations of the NCAR global circulation model. *Mon. Wea. Rev. 104*, 1372–1391.